p-ISSN 0852 – 0798
e-ISSN 2407 – 5973

Website: http://ejournal.undip.ac.id/index.php/reaktor/

Reaktor, Vol. XX No. X, Month Year XXXX, pp. Xxx-xxx

Comparative Simulation and Modeling of Hydrogen Explosion Consequences based on TNT Equivalent

Virda Nur Lu'lu [1,2)], Pramujo Widiatmoko [1,2)], Hary Devianto [1,2*)]

[1)] Department of Chemical Engineering, Faculty of Industrial Technology, Institut Teknologi Bandung
Jalan Ganesha No.10, Bandung 40132, Indonesia
[2)]Laboratory of Energetic Process and Electrochemical Safety Laboratory, Institut Teknologi Bandung
Jalan Ganesha No.10, Bandung 40132, Indonesia

[*)] Corresponding author: hardev@itb.ac.id

(Received: xx xx xxxx; Accepted: xx xx xxxx; Published: xx xx xxxx)

Abstract

Hydrogen is increasingly adopted as a low-carbon energy carrier, creating a need for rapid and auditable blast-consequence screening to inform hazard zoning. This study develops a web-based simulation platform that automates a transparent TNT-equivalent workflow from minimal inputs (inventory volume and evaluation distance). The platform converts volume to mass, estimates TNT-equivalent charge using an energy basis and efficiency factor, applies Hopkinson–Cranz cube-root scaling, and predicts peak side-on overpressure using three published correlations (Crowl and Louvar, Alonso, and Sadovski) under harmonized assumptions, while exporting calculation logs for traceability. Validation uses a Type-IV high-pressure hydrogen vessel-burst dataset with measurements at 2–18 m. Over the sensor-intact 6–18 m window, Alonso achieves MAE 6.006 kPa with R^2 0.999, whereas Crowl and Louvar and Sadovski yield MAEs of 18.136 kPa and 17.164 kPa with R^2 of 0.985 and 0.993. A 50 kg TNT-equivalent Gangneung 2019 plausibility case gives 50.9–86.7 kPa at 15 m and 3.58–6.34 kPa at 100 m, consistent with reported steel deformation and widespread glazing damage. Overall, the platform enables transparent, traceable preliminary consequence estimation to support hazard-zoning decisions for hydrogen storage.

Keywords: Blast consequence screening; Hopkinson–Cranz scaling; Hydrogen explosion; Peak side-on overpressure; TNT equivalent

How to Cite This Article: Virda Nur Lu'lu, Pramujo Widiatmoko, Hary Devianto (2026), Comparative Simulation and Modeling of Hydrogen Explosion Consequences based on TNT Equivalent, Reaktor, xx (x), xx - xx, https://doi.org/10.14710/reaktor. xx. x. xx - xx

INTRODUCTION

Hydrogen (H_2) is increasingly positioned as a low-carbon energy carrier, accelerating the deployment of production, storage, distribution, and refuelling infrastructure (Ma et al., 2024). Global hydrogen demand exceeded 97 Mt in 2023 and is projected to approach 100 Mt in 2024, while uptake in new clean energy applications remains below 1% of total demand, implying rapid infrastructure expansion and increasing inventory exposure across the value chain (International Energy Agency (IEA), 2024). In

facility design and operation, this trend reinforces the need for fast and defensible separation distance decisions and consequence screening, particularly where hydrogen assets are located near critical infrastructure and occupied areas (Joshi et al., 2024; LaChance, 2009).

Hydrogen explosion hazards remain central to process safety because hydrogen exhibits a wide flammability range in air from 4 to 75% by volume and a very low minimum ignition energy of about 0.02 mJ, meaning ignition can be initiated by weak ignition sources under certain mixing conditions (Calabrese et al., 2024; Suwa, 2024). Incident statistics further highlight practical relevance, as Hydrogen Incident Database reports 120 hydrogen incidents from 1999 to 2019, dominated by laboratory events at 38.3%, followed by refueling stations at 10.6% and commercial zones at 9.0% (Yang et al., 2021). A notable large-scale example is the Gangneung incident (South Korea, May 2019), where a pressure-vessel system used for elektroliser testing exploded with a reported blast equivalent of 50 kg TNT (CHS, 2019), resulting in two fatalities, six injuries, and severe damage to nearby facilities (Cekerevac and Cekerevac, 2025). Such incidents demonstrate that vessel scenarios can generate blast loads sufficient to threaten building integrity and human safety, motivating practical methods to delineate hazard zones for layout design and emergency planning (Stolecka-Antczak et al., 2024; Zhou et al., 2024).

High-fidelity consequence assessment for hydrogen explosions is typically pursued via dedicated experiments and Computational Fluid Dynamics (CFD), but both are costly and time-consuming (Min and Kang, 2024). Commercial integral-model software such as DNV Phast is widely used in industry for explosion consequence analysis, but access can be constrained by licensing requirements and dependence on dedicated software ecosystems (DNV, 2024). As a practical option for early-stage decision-making, the TNT-equivalent approach remains widely applied as a screening method to estimate peak side-on overpressure from scaled-distance relationships for parametric studies, preliminary protection evaluation, and safety-distance determination (Crowl and Louvar, 2011; Han et al., 2025). To address this need, this study develops a web-based hydrogen explosion simulation platform that automates the TNT-equivalent workflow from minimal inputs of inventory volume and evaluation distance, implements three established empirical correlations from Crowl and Louvar, Alonso, and Sadovski under harmonized assumptions, and generates peak side-on overpressure as a function of distance. The platform is first validated against instrumented pressure vessel burst datasets reported in the literature to confirm that the predicted overpressure decay with distance is reproduced within the measurement-supported range, and it is subsequently transferred to the Gangneung 2019 case as a field-scale plausibility check (Cekerevac and Cekerevac, 2025; CHS, 2019; Han et al., 2025). Following the validation step, the platform provides peak side-on overpressure predictions at the evaluated distances as a preliminary screening output to support early-stage safety-distance interpretation for hydrogen storage scenarios.

METHODOLOGY

A TNT-equivalent method was used to estimate the peak side-on overpressure (P_o) for hydrogen (H_2) explosion scenarios. Three empirical formulations of Crowl and Louvar, Alonso, and Sadovski were implemented within a single computational workflow and executed in parallel under identical scenario inputs (Fig. 1), allowing direct comparison of the predicted overpressure under consistent assumptions. The implementation records the full calculation trail (inputs, intermediate scaled variables, and model-specific outputs) and exports the run log in a tabular format to support traceability and independent recalculation.

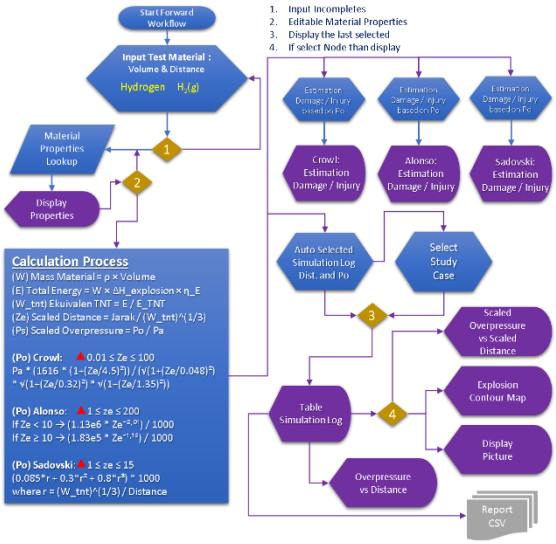

Figure 1. Workflow of the TNT equivalent simulation platform integrating Crowl & Louvar, Alonso, and Sadovski for peak side-on overpressure estimation

TNT Equivalent Workflow

The inventory mass was determined for each scenario, as determined by Eq. (1).

$$W = \rho \cdot V \tag{1}$$

where W is inventory mass (kg), ρ is density of the inventory ($\mathrm{kg \cdot m^{-3}}$), and V is inventory volume ($\mathrm{m^3}$).

The total energy of the explosive material can be determined using Eq. (2).

$$E_{total} = W \cdot \Delta H_{exp} \cdot \eta \tag{2}$$

where ΔH_{exp} is explosion energy of the explosive material (with hydrogen's heat of explosion being 130800 kJ/kg) and η is explosion efficiency factor representing total energy of the explosive material converted into blast loads. The η value is empirical and contingent upon the conditions of the release of the explosion, ignition sources, and environmental factors. The η value of hydrogen explosions varies from 1% to 10% (Han et al., 2025; Lees, 2012). The equivalent mass of the TNT is calculated based on the total energy released during an explosion using Eq. (3) (Crowl and Louvar, 2011).

$$W_{TNT} = \frac{E_{total}}{E_{TNT}} \quad (3)$$

where W_{TNT} is the TNT equivalent mass (kg), E_{TNT} is the explosion energy of TNT within the range of 4230−4836 kJ/kg (Wang et al., 2023). The W_{TNT} value is utilized to calculate the scaled distance according to the Hopkinson-Cranz scaling law or cube-root law using Eq. (4) (Crowl and Louvar, 2011).

$$Z_e = \frac{R}{W_{TNT}^{1/3}} \quad (4)$$

where Z_e is the scaled distance $\left(\mathrm{m} \cdot \mathrm{kg}^{-1/3}\right)$, R is the distance from the explosion center (m). The Hopkinson–Cranz scaling law states that, for a given explosive and detonation configuration, blast overpressure responses are expected to be comparable when evaluated at the same scaled distance, even for different charge weights (Wei and Hargather, 2021).

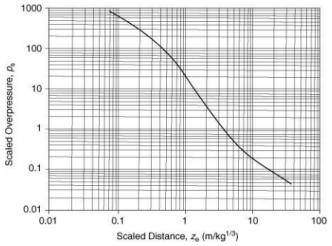

Figure 2. Scaled Distance (Z_e) vs Scaled Overpressure (P_s)

Scaled overpressure (P_s) is the ratio of peak side-on overpressure (P_o) in kPa to ambient pressure (P_a) of 101.325 kPa, as expressed in Eq. (5) and Fig 2.

$$P_s = \frac{P_o}{P_a} \quad (5)$$

Empirical Peak Side-on Overpressure Correlations

The three correlations were developed from different experimental bases and therefore differ in applicability range and fitted curve characteristics.

Crowl & Louvar's methodology

Crowl & Louvar (2011) implement the Kinney–Graham correlation for TNT surface bursts on a flat surface, as determined by Eq. (6).

$$\frac{P_o}{P_a} = \frac{1616\left[1+\left(\frac{Ze}{4.5}\right)^2\right]}{\sqrt{\left[1+\left(\frac{Ze}{0.048}\right)^2\right]}\sqrt{\left[1+\left(\frac{Ze}{0.32}\right)^2\right]}\sqrt{\left[1+\left(\frac{Ze}{1.35}\right)^2\right]}} \quad (6)$$

In this study, results at low scaled distances are treated with caution because empirical blast correlations typically show larger dispersion in the near field (e.g., $0.2 \leq Z_e \leq 1$) and become more stable for $Z_e \geq 1$ (Ullah et al., 2017). Values outside the adopted interpretation range are flagged as extrapolative screening outputs.

Alonso's methodology

The Alonso correlation provides $P_o$as a power-law function of Z_e over two validity ranges (Díaz Alonso et al., 2006).

For $1 \leq Z_e < 10$ can be calculated by Eq. (7) as follows:

$$P_o = 1.13 \times 10^6 \, Z_e^{(-2,01)} \quad (7)$$

For $10 \leq Z_e \leq 200$ can be determined by Eq. (8) as follows:

$$P_o = 1.83 \times 10^5 \, Z_e^{(-1,16)} \quad (8)$$

where P_o is obtained in Pascals (Pa) and is converted to kilopascals (kPa) for reporting. Predictions outside $1 \leq Z_e \leq 200$ are labelled as extrapolated.

Sadovski's methodology

The Sadovski formulation estimates P_o based on empirical TNT blast tests and assumes a pseudo-spherical blast origin(Jeremić and Bajić, 2006), as expressed in Eq. (9).

$$P_o = 0.085 \frac{\sqrt[3]{W_{TNT}}}{R} + 0.3\left(\frac{\sqrt[3]{W_{TNT}}}{R}\right)^2 + 0.8\left(\frac{\sqrt[3]{W_{TNT}}}{R}\right)^3 \quad (9)$$

where P_o is obtained in MPa and converted to kPa for reporting. This study applies Sadovski within $1 \leq Z_e \leq 15$ (Jankura et al., 2020), while values outside this range are flagged as extrapolative.

Consequences Classification Based on Peak Side-on Overpressure

Blast consequences were assessed by mapping the predicted peak side-on overpressure (P_o) to threshold-based impact categories for structural damage and human injury severity (Crowl and Louvar, 2011; Jeremić and Bajić, 2006; Wang et al., 2023). In this study, consequence classification is reported in terms of P_o as a screening-level metric, consistent with simplified damage criteria that relate peak overpressure to hazard zoning and preliminary safety-distance interpretation. Accordingly, the predicted P_o values at each radial distance were translated into qualitative consequence classes using compiled threshold ranges from multiple literature sources

summarised in Tables 1 and 2, while the full classification criteria and source attribution are provided in Supplementary Tables S1 and S2.

Table 1. Summary of structural damage classification thresholds based on peak side-on overpressure

Impact category	P_o range (kPa)	Short descriptor
IC1 Insignificant	0.14–2	Glazing effects and incidental glass damage
IC2 Minor	>2–9	Minor glass breakage and light architectural damage
IC3 Moderate	>9–25	Widespread glazing failure and major non-structural damage
IC4 Serious	>25–40	Extensive non-structural damage and severe building impairment
IC5 Severe	>40–55	Heavy damage with high likelihood of ceiling and facade collapse
IC6 Major	>55–76	Major damage including impacts to load-bearing components
IC7 Catastrophic	>76	Near-total collapse of building elements

Table 2. Summary of human injury classification thresholds based on peak side-on overpressure

Impact category	P_o range (kPa)	Short descriptor
IC1 Minor injury	<20	Primary blast injury unlikely, secondary injury possible
IC2 Moderate injury	20–30	Minor contusion and low eardrum-rupture likelihood
IC3 Serious injury	30–50	Injury severity increases due to combined blast and debris effects
IC4 Severe injury	50–100	Severe injury risk with potential fatality depending on exposure
IC5 Fatality	>100	High fatality likelihood for unprotected individuals

Validation Scenarios

The platform performance was evaluated using two complementary validation scenarios, namely a controlled pressure vessel burst dataset and a field benchmark event. The essential input parameters adopted for both cases are summarized in Table 3.

Baseline PVBs scenario

The baseline validation case was adopted from the Type-IV high-pressure hydrogen pressure vessel burst dataset reported by Han et al. (2025), where peak side-on overpressure was measured at distances of 2–18 m from the explosion center and mapped to TNT reference responses with additional refinement using CFD simulations. The dataset represents an open-field configuration, with the ground as the only reflecting boundary. In the reference study, TNT charge weights were designed using an energy-based TNT equivalency framework by considering the commonly reported explosion-efficiency range of 1–10% and selecting three representative values of $\eta = 3.5\%$, 5.5%, and 7.0% to support the experimental matching campaign. Using a hydrogen inventory of 7.15 kg and the adopted energy constants of 130800 kJ/kg for hydrogen and 4520 kJ/kg for TNT, TNT charge weights were evaluated at the same measurement locations as the hydrogen experiment (2, 4, 6, 8, 10, 14, and 18 m) to establish distance-dependent peak overpressure equivalence. Following the experimental–computational matching, a calibrated TNT-equivalent mass of 9.53 kg with a corresponding yield factor of 0.046 was reported, and these calibrated parameters were adopted directly in this study so that the platform inputs rely on a measurement-anchored TNT equivalency rather than an assumed or tuned efficiency.

For thermophysical consistency, hydrogen properties were evaluated in Aspen HYSYS using the hydrogen-suitable MBWR package as the equation of state (Rezaie Azizabadi et al., 2021). The inventory density was taken from the reported vessel charge ($\rho = 40.86$ kg/m³) and cross-checked at the rupture pressure (79.8 MPa) in Aspen HYSYS v14 (2023) using MBWR. The bulk temperature was iteratively adjusted until the EOS reproduced the inventory-based density, yielding an EOS-consistent state of T = 46.86 °C with a non-ideal compressibility factor of $Z = 1.4$.

Field-scale plausibility case (R&D Gangneung 2019)

After validation against the PVBs dataset, the platform was further assessed using the hydrogen tank explosion that occurred in Gangneung, South Korea, in May 2019 as a field-scale plausibility case. A technical review by the Center for Hydrogen Safety estimated the event to be equivalent to approximately 50 kg TNT and reported no secondary fire, indicating that the observed consequences were primarily blast driven. The same review described severe near-field damage at around 15 m and widespread window breakage at approximately 100 m (CHS, 2019). In this study, the Gangneung scenario was represented using the reported tank capacity and operating pressure together with ambient conditions, with the ambient temperature taken as approximately 31 °C based on historical weather records for Gangneung in May 2019 (“Past Weather in Gangneung, South Korea — May 2019,” 2019). Hydrogen density at 1 MPa and the adopted ambient temperature was cross-checked in Aspen HYSYS (2023) using the hydrogen suitable MBWR package, yielding $\rho = 0.793$ kg/m³ with a

Table 3.Validation scenarios for hydrogen explosions, including essential input parameters

Properties	H_2 explosion experiment	R&D Gangneung H_2 tank explosion
Density, ρ (kg/m^3)	40.86	0.793
Volume, V (m^3)	0.175	40
Heat of explosion, ΔH_{exp} (kJ/kg)	130800	130800
Explosion energy of TNT, E_{TNT} (kJ/kg)	4520	4520
Efficiency (η)	0.046	0.055

near-ideal compressibility factor of $Z = 1.006$. To preserve consistency with the baseline energy-based TNT-equivalency framework, the explosion efficiency for the Gangneung case was not introduced as an independent tuning parameter. Instead, the efficiency was back calculated as 0.055 (5.5%) so that the reported field equivalence of 50 kg TNT is reproduced under the adopted hydrogen inventory and the same energy constants used in the baseline case.

RESULTS AND DISCUSSION

Pressure Vessel Bursts (PVBs) Baseline Validation

Peak side-on overpressure data for the baseline PVB validation in this study were adopted from the Type-IV hydrogen pressure vessel burst experiments reported by Han et al.(2025). The measured response exhibits a pronounced decay with distance, decreasing from 1238.98 kPa at $R = 2$m to 23.17 kPa at $R = 18$m. The reference study also noted near-field measurement limitations, where the 2 m and 4 m sensors were damaged after capturing the peak overpressure value, resulting in comparatively noisier signals at these locations than at the remaining measurement points.

As summarized in Table 4, the three TNT-equivalent correlations (Crowl and Louvar, Alonso, and Sadovski) reproduce the distance-dependent attenuation of measured peak side-on overpressure, while the predicted pressure levels differ across evaluation distances. At $R = 2$ m ($Z_e = 0.94$), Crowl and Louvar yields a markedly higher estimate (2287.41 kPa, +85%), whereas Alonso provides the closest agreement (1270.59 kPa, +3%) and Sadovski gives 1380.24 kPa (+11%). At $R = 4$ m ($Z_e = 1.89$), Crowl and Louvar remain above the measurement (+18%), while Alonso and Sadovski underpredict (−22% and −38%). Over the sensor-intact window of 6–18 m, Crowl and Louvar continues to overpredict but with a progressively smaller deviation (+42% at 6 m to +8% at 18 m), whereas Alonso and Sadovski are predominantly below the measurements and converge to similar values at the longest evaluation distance (−34% and −33% at 18 m). These pointwise deviations indicate that, under harmonised TNT-equivalent inputs, screening distances inferred at a specified P_o criterion can vary across formulations.

In Figure 3. presents platform-generated baseline-validation visualizations in both scaled-distance coordinates and peak overpressure versus evaluation distance, enabling cross-correlation differences to be examined under a consistent TNT-equivalent basis. Across the evaluated window, inter-model dispersion is more pronounced at lower scaled distances ($0.2 < Z_e < 1.0$), and whereas the variation becomes much smaller for $Z_e > 1.0$, indicating that the empirical relations tend to converge more closely in the larger-scaled-distance regime (Ullah et al., 2017). In the present dataset, only the $R = 2$ m point yields $Z_e < 1$, whereas the remaining points ($R = 4$–18 m) correspond to $Z_e > 1$, consistent with tighter clustering of predictions as Z_e increases. Accordingly, the platform applies Z_e-based validity alarms and prioritizes screening interpretation in the higher-Z_e regime, while results at lower Z_e are interpreted with additional caution. This treatment aligns with broader discussions that TNT-equivalent screening tends to be more dependable at larger distances, whereas close-range predictions are more sensitive to uncertainties in the effective source representation and the fraction of release energy converted into blast loading (Chen et al., 2023).

Overall predictive performance over the evaluation window was summarized using the mean absolute error (MAE) and the coefficient of determination (R^2). MAE quantifies the average absolute deviation between measured and predicted peak side-on overpressures, whereas R^2 indicates how well the models reproduce the distance-dependent attenuation pattern across the evaluated distances. Because MAE is based on absolute deviations, it does not retain the sign of the residuals; therefore, the direction of the pointwise errors reported in Table 4 was examined in parallel when interpreting conservatism for screening applications (Khoshvaght et al., 2025). The statistics were calculated over the sensor-intact window of 6–18 m (6, 8, 10, 14, and 18 m) to remain consistent with the reliability window adopted in the reference dataset and to avoid overweighting the close-range regime. For each evaluation distance, the measured value is denoted by $y_i$and the corresponding model prediction is denoted by x_i. MAE was calculated as the average absolute deviation across n distances (Eq. 10), and R^2 was calculated from the residual and total sums of squares (Eq. 11), where $\bar{y}$ denotes the meaning of the measured values.

Table 4. Deviation of TNT-equivalent predictions from measured peak side-on overpressure in the Type-IV hydrogen PVBs case

Distance, R (m)	P_o, exp (kPa)	Z_e (m·kg$^{-1/3}$)	Crowl & Louvar		Alonso		Sadovski	
			P_o (kPa)	Error (%)	P_o (kPa)	Error (%)	P_o (kPa)	Error (%)
2	1238.98	0.94	2287.412	85	1270.585	3	1380.244	11
4	403.57	1.89	476.485	18	315.452	-22	248.461	-38
6	132.37	2.83	187.462	42	139.634	5	102.791	-22
8	79.26	3.77	100.973	27	78.318	-1	58.488	-26
10	56.25	4.72	65.132	16	50.012	-11	39.13	-30
14	33.19	6.6	36.387	10	25.431	-23	22.531	-32
18	23.17	8.49	24.966	8	15.345	-34	15.481	-33

Notes: (1) Positive error indicates overprediction; (2) negative error indicates underprediction

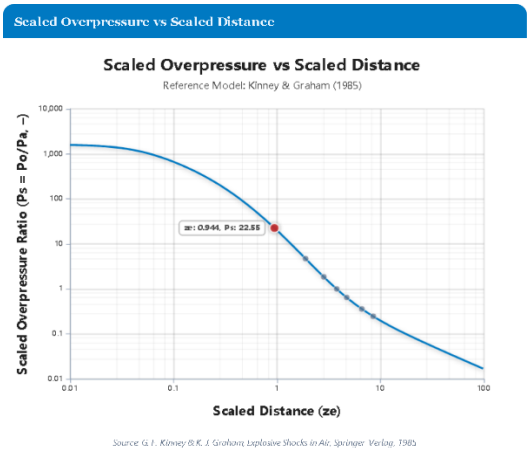

(a) Scaled overpressure as a function of scaled distance

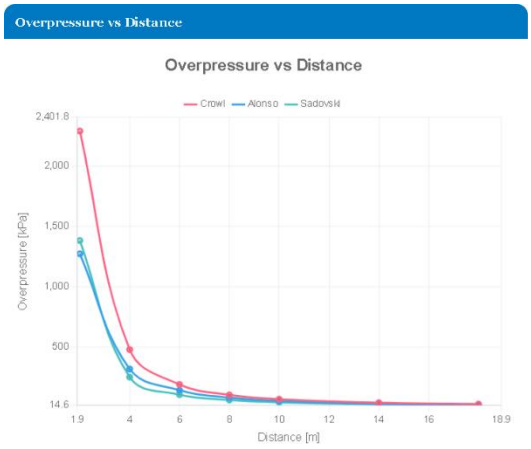

(b) Predicted peak side-on overpressure versus distance or cross-correlation comparison.

Figure 3. Platform-generated baseline PVBs validation visualization against Type-IV hydrogen pressure vessel burst measurements

$$MAE = \frac{1}{n}\sum_{i=1}^{n}|y_i - x_i| \quad (10)$$

$$R^2 = 1 - \frac{\sum_{i=1}^{n}(y_i - x_i)^2}{\sum_{i=1}^{n}(y_i - \bar{y})^2} \quad (11)$$

Over 6–18 m, Alonso gives the lowest MAE (6.006 kPa) with $R^2 = 0.999$, while Crowl and Louvar and Sadovski yield MAEs of 18.136 kPa and 17.164 kPa with R^2 values of 0.985 and 0.993, respectively. The uniformly high R^2 values confirm that all three correlations represent the attenuation pattern well over the evaluated window; the practical distinction is therefore dominated by magnitude agreement and error direction. In this dataset, Crowl and Louvar provides consistently higher estimates over 6–18 m with decreasing deviation at larger distances, supporting its use as a conservative screening curve, whereas Alonso provides the closest numerical agreement but remains below the measurements at several Z_e>1 points and is therefore better positioned as a best-fit reference or as a comparative curve alongside a conservative envelope.

Transferability of the Calibrated PVBs Baseline to a Real Event: Gangneung 2019

The calibrated PVB baseline was transferred to the Gangneung 2019 field-scale plausibility case by matching the Hopkinson–Cranz scaled distance (Z_e), so that comparable blast overpressure responses are inferred on a consistent TNT-equivalent basis. Under this principle, blast responses from different charge weights can be compared when evaluated at the same scaled distance (Wei and Hargather, 2021).

In this study, the Gangneung 2019 incident was represented as a field-scale plausibility case with an estimated equivalence of approximately 50 kg TNT, with consequences dominated by blast effects and without a dominant secondary fire. By retaining the baseline $Z_e$values, each baseline radial evaluation distance (R) was mapped to an adjusted field distance (R_{adj}) for the 50 kg charge using Eq. (12). This mapping yields some correspondence from 2–18 m in the baseline case to approximately 3.48–31.30 m as shown in Table 5.

$$R_{adj} = Z_e \cdot W_{TNT}^{1/3} \quad (12)$$

The mapped field distances and the corresponding peak side-on overpressures predicted by Crowl & Louvar, Alonso, and Sadovski are reported in Table 5. Internal numerical consistency was checked by comparing, for each correlation, the scaled-up prediction evaluated at R_{adj} and the

baseline prediction evaluated at the same Z_e. The resulting deviations remain within −0.27% to 0.10% across the mapped points, indicating that the scale-transfer step preserves the intended cube-root scaling behaviour, with residual differences attributable to rounding and floating-point precision. These deviations are well below the 1% magnitude commonly reported for simulator-to-benchmark comparisons in chemical engineering, supporting internal consistency of the scale-up implementation (Andreasen, 2022).

Consequence Interpretation Based on Structural and Human-Injury Thresholds

Following verification of the scale-transfer consistency, the predicted peak side-on overpressure P_o for the Gangneung 2019 plausibility case (TNT-equivalent mass of 50 kg) was interpreted using threshold-based consequence zoning. Predictions from Crowl and Louvar, Alonso, and Sadovski were mapped to the structural impact categories in Table 1 (IC1–IC7) and the human-injury categories in Table 2 (IC1–IC5). The three correlations are presented in parallel to quantify inter-correlation spread, while a conservative zoning interpretation is obtained by referencing the upper-bound P_o at each evaluation distance to avoid delineating buffer zones using lower estimates. The spatial distribution of P_o is additionally summarised by the platform-generated contour map in Fig. 4(a), where the source location is specified by input coordinates (37.805070° N, 128.856997° E) adopted from the R&D Gangneung site marker in Google Maps; this coordinate input places the explosion centre on the basemap so that contour zones can be interpreted directly against evaluation distances.

Consistency with reported field effects was assessed using two qualitative indicators documented by the Center for Hydrogen Safety, namely structural steel member deformation at approximately 15 m and extensive window breakage at approximately 100 m (CHS, 2019), supported by post-incident photographs in Fig. 4(b)–(c). At 15 m ($Z_e = 4.06$ m·kg$^{-1/3}$), the predicted overpressure is 51.1 kPa (Sadovski), 67.6 kPa (Alonso), and 87.1 kPa (Crowl and Louvar), mapping to IC5–IC7 in Table 1. This band corresponds to severe-to-catastrophic structural impact categories, which is compatible with the reported deformation of steel members at that distance; within the three predictions, Alonso falls within the IC6 interval while Crowl and Louvar provides the conservative envelope (IC7). At 100 m ($Z_e = 27.06$ m·kg$^{-1/3}$), predicted overpressure decreases to 6.36 kPa (Crowl and Louvar), 3.99 kPa (Alonso), and 3.59 kPa (Sadovski), mapping to IC2 in Table 1, a regime dominated by facade and glazing damage rather than load-bearing failure, consistent with the reported widespread window breakage. For this distance, the platform flags the Sadovski result as extrapolative because Z_e exceeds its stated validity range; therefore, interpretation can preferentially reference Alonso for alignment with the correlation's validity window while retaining Crowl and Louvar as the conservative upper bound for buffer-zone screening.

For human-injury interpretation, the 15 m predictions (51.1–87.1 kPa) map to IC4 in Table 2. (50–100 kPa), which denotes a severe-injury regime with potential fatality for unprotected exposure under peak-overpressure threshold schemes (Crowl and Louvar, 2011; Jeremić and Bajić, 2006; Wang et al., 2023). At 100 m, the predicted peak side-on overpressures (3.6–6.4 kPa) remain within IC1 (<20 kPa), where primary blast injury is unlikely; consequence interpretation is therefore driven mainly by secondary/tertiary injury pathways associated with facade and glazing damage, consistent with the IC2 structural classification at the same distance. Public reporting of the Gangneung incident indicates fatalities and injuries but does not provide verified exposure distances; accordingly, the injury discussion in this study is presented as a threshold-based plausibility check for zoning interpretation, rather than a distance-calibrated validation of casualty outcomes.

CONCLUSION

This study delivers a web-based simulation platform that automates a transparent TNT-equivalent workflow for hydrogen consequence screening, enabling traceable calculation from inventory inputs to Hopkinson–Cranz scaling and peak side-on overpressure prediction using multiple empirical correlations. Internal verification of the scale-transfer implementation from the calibrated pressure-vessel-burst baseline to the Gangneung plausibility case shows deviations confined to −0.27% to 0.10%, confirming numerically consistent implementation with differences dominated by precision and rounding.

Against the Type-IV hydrogen pressure vessel burst dataset, all correlations reproduce the attenuation pattern over the sensor-intact 6–18 m window. Alonso provides the closest agreement (MAE 6.006 kPa; R^2 0.999), whereas Crowl and Louvar yields higher estimates with decreasing deviation at larger evaluation distances, supporting its use as a conservative screening envelope when buffer-zone definition must avoid reliance on lower predictions.

For the Gangneung plausibility case, predicted overpressures at approximately 15 m map to major-to-catastrophic structural impact categories and a severe injury band for unprotected exposure, while values at approximately 100 m fall in a glazing-dominated damage regime with low likelihood of primary blast injury but credible secondary injury potential from glass fragments.

Table 5. Hopkinson–Cranz scale-up consistency from the PVBs baseline to the Gangneung benchmark using adjusted distance (R_{adj})

R (m)	Z_e (m·kg$^{-1/3}$)	R_{adj} (m)	P_o (kPa) at W_{TNT} 50 kg			Error (%)		
			Crowl	Alonso	Sadovski	Crowl	Alonso	Sadovski
2	0.94	3.48	2282.466	1268.002	1376.581	-0.22%	-0.20%	-0.27%
4	1.89	6.95	476.954	315.719	248.702	0.10%	0.08%	0.10%
6	2.83	10.43	187.438	139.618	102.779	-0.01%	-0.01%	-0.01%
8	3.77	13.91	100.912	78.272	58.455	-0.06%	-0.06%	-0.06%
10	4.72	17.39	65.148	50.025	39.14	0.02%	0.03%	0.03%
14	6.60	24.34	36.376	25.421	22.524	-0.03%	-0.04%	-0.03%
18	8.49	31.30	24.964	15.344	15.48	-0.01%	-0.01%	-0.01%

Notes: (1) Positive error indicates overprediction; (2) negative error indicates underprediction

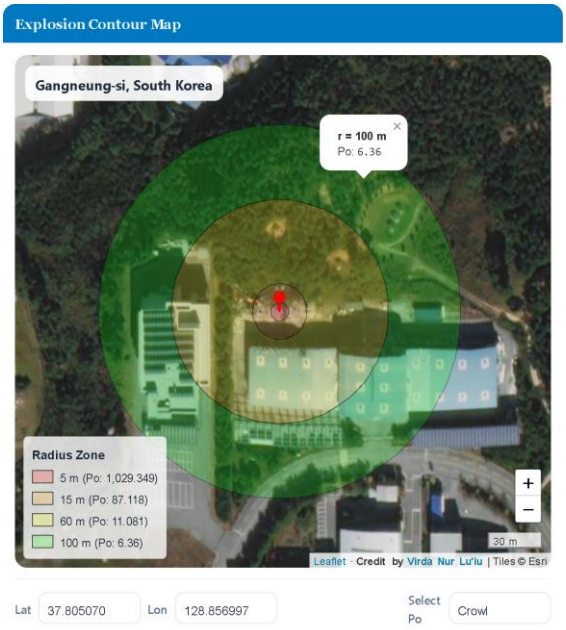

(a) Platform-generated peak side-on overpressure (P_o) contour map for the Gangneung 2019 plausibility case (50 kg TNT equivalent)

(b) Near-field structural damage observed at approximately 15 m

(c) Far-field facade damage observed at approximately 100 m

Figure 4. Field-scale consequence interpretation for the Gangneung 2019 benchmark at 50 kg TNT equivalent (Chang-won, 2019; Times, 2019)

Future work will prioritize strengthening the screening credibility of the TNT-equivalent platform through broader multi-scenario validation for hydrogen explosion using additional instrumented datasets and field benchmarks, supported by a structured parameter database for key assumptions, particularly the case-dependent efficiency factor, to enable sensitivity- and uncertainty-aware screening outputs. The platform framework will then be extended to additional hazardous materials so that

cross-material consequence screening can be performed under harmonized assumptions and consistent reporting.

NOTATION

Latin Letters	
E	Total explosion energy of hydrogen (kJ)
E_{TNT}	Explosion energy of TNT (kJ/kg)
MAE	Mean absolute error (kPa)
W	Hydrogen inventory mass (kg)
n	Number of evaluation data points (–)
P_a	Ambient pressure (kPa)
P_o	Peak side-on overpressure (kPa)
P_o, exp	Peak side-on overpressure, experiment (kPa)
R	Radial distance from explosion center (m)
R_{adj}	Adjusted radial distance after scaling (m)
R^2	Coefficient of determination (–)
T	Temperature (°C as specified)
V	Hydrogen inventory volume (m³)
W_{TNT}	Equivalent TNT mass (kg)
x_i	Predicted peak side-on overpressure at data point *i* (kPa)
y_i	Measured peak side-on overpressure at data point *i* (kPa)
$\bar{y}$	Mean of measured peak side-on overpressure values (kPa)
Z	Compressibility factor (–)
Z_e	Scaled distance (m·kg$^{-1/3}$)
Greek Letters	
η	Explosion efficiency factor (–)
ρ	Hydrogen density (kg/m³)
ΔH_{exp}	Specific explosion energy of hydrogen (kJ/kg)

CONFLICT OF INTEREST

The authors confirm that there are no conflicts of interest

ACKNOWLEDGEMENTS

The author gratefully acknowledges the supervision and academic guidance provided throughout this research. The author also acknowledges the researchers whose published datasets and incident summaries enabled the validation framework applied in this study.

REFERENCES

Andreasen, A., 2022. Evaluation of an Open-source Chemical Process Simulator Using a Plant-wide Oil and Gas Separation Plant Flowsheet Model as Basis. Period. Polytech. Chem. Eng. 66, 503–511. https://doi.org/10.3311/PPch.19678

Aspen Technology, Inc., 2023. Aspen Hysys.

Calabrese, M., Portarapillo, M., Di Nardo, A., Venezia, V., Turco, M., Luciani, G., Di Benedetto, A., 2024. Hydrogen Safety Challenges: A Comprehensive Review on Production, Storage, Transport, Utilization, and CFD-Based Consequence and Risk Assessment. Energies 17, 1350. https://doi.org/10.3390/en17061350

Cekerevac, Z., Cekerevac, D., 2025. HYDROGEN HAZARDS, RISKS, AND PROTECTION: AN IN-DEPTH REVIEW. MEST J. 13, 23–48. https://doi.org/10.12709/mest.13.13.SP.02

Chang-won, L., 2019. Explosion at hydrogen fuel-cell power system kills two and injuries six others. AJP News Agency.

Chen, D., Wu, C., Li, J., 2023. Assessment of modeling methods for predicting load resulting from hydrogen-air detonation. Process Saf. Environ. Prot. 180, 752–765. https://doi.org/10.1016/j.psep.2023.10.051

CHS, C. for H.S., 2019. Review: Hydrogen Tank Explosion in Gangneung, South Korea. Presented at the 2019 Center for Hydrogen Safety Conference, AIChE (American Institute of Chemical Engineers).

Crowl, D.A., Louvar, J.F., 2011. Chemical process safety: fundamentals with applications, 3rd ed. ed, Prentice Hall international series in the physical and chemical engineering sciences. Prentice Hall, Upper Saddle River, NJ.

Díaz Alonso, F., González Ferradás, E., Francisco Sánchez Pérez, J., Miñana Aznar, A., Ruiz Gimeno, J., Martínez Alonso, J., 2006. Characteristic overpressure–impulse–distance curves for the detonation of explosives, pyrotechnics or unstable substances. J. Loss Prev. Process Ind. 19, 724–728. https://doi.org/10.1016/j.jlp.2006.06.001

DNV, 2024. Phast™: Fire, Explosion, Dispersion, and Toxic Modeling Software. DNV.

Han, S., Baek, S.-H., Jeon, Y., Kim, K., Park, S., 2025. Integrated experimental-computational approach to estimate TNT equivalence of hydrogen vessel bursts. Int. J. Hydrog. Energy 146, 149936. https://doi.org/10.1016/j.ijhydene.2025.06.126

International Energy Agency (IEA), 2024. Global Hydrogen Review 2024. International Energy Agency.

Jankura, R., Zvaková, Z., Boroš, M., 2020. ANALYSIS OF MATHEMATICAL RELATIONS FOR CALCULATION OF EXPLOSION WAVE OVERPRESSURE. Proc. CBU Nat. Sci. ICT 1, 21–27. https://doi.org/10.12955/pns.v1.116

Jeremić, R., Bajić, Z., 2006. An approach to determining the TNT equivalent of high explosives. Sci.-Tech. Rev. LV, 58–62.

Joshi, A., Sattari, F., Lefsrud, L., Tufail, M., Khan, M.A., 2024. Mitigating uncertainty: A risk informed approach for deploying hydrogen refueling stations. Int. J. Hydrog. Energy 74, 136–150. https://doi.org/10.1016/j.ijhydene.2024.06.085

Khoshvaght, H., Permala, R.R., Razmjou, A., Khiadani, M., 2025. A critical review on selecting performance evaluation metrics for supervised machine learning models in wastewater quality prediction. J. Environ. Chem. Eng. 13, 119675. https://doi.org/10.1016/j.jece.2025.119675

LaChance, J., 2009. Risk-informed separation distances for hydrogen refueling stations. Int. J. Hydrog. Energy 34, 5838–5845. https://doi.org/10.1016/j.ijhydene.2009.02.070

Lees, F., 2012. Lees' Loss Prevention in The Process Industries, Fourth Edition. ed.

Ma, Q., Guo, Y., Zhong, M., Ya, H., You, J., Chen, J., Zhang, Z., 2024. Numerical simulation of hydrogen explosion characteristics and disaster effects of hydrogen fueling station. Int. J. Hydrog. Energy 51, 861–879. https://doi.org/10.1016/j.ijhydene.2023.05.129

Min, H., Kang, H., 2024. Prediction of a Hydrogen Vapor Cloud Explosion with a Barrier Wall Using Various Machine Learning Methods. Processes 12, 2946. https://doi.org/10.3390/pr12122946

Past Weather in Gangneung, South Korea — May 2019, 2019.

Rezaie Azizabadi, H., Ziabasharhagh, M., Mafi, M., 2021. Applicability of the common equations of state for modeling hydrogen liquefaction processes in Aspen HYSYS. Gas Process. J. 9. https://doi.org/10.22108/gpj.2020.123736.1087

Stolecka-Antczak, K., Rusin, A., Kosman, W., Rusin, K., Paltrinieri, N., 2024. Hazards Caused By Hydrogen Explosion At Refueling Station Due To Uncontrolled Gas Release.

Suwa, Y., 2024. Studies on the safe application techniques of high-pressure hydrogen gas. J. Phys. Conf. Ser. 2812, 012002. https://doi.org/10.1088/1742-6596/2812/1/012002

Times, 2019. Hydrogen tank explosion kills 2 in Gangneung.

Ullah, A., Ahmad, F., Jang, H.-W., Kim, S.-W., Hong, J.-W., 2017. Review of analytical and empirical estimations for incident blast pressure. KSCE J. Civ. Eng. 21, 2211–2225. https://doi.org/10.1007/s12205-016-1386-4

Wang, Q., Zhang, L., Wang, L., Bu, L., 2023. A practical method for predicting and analyzing the consequences of ammonium nitrate explosion accidents adjacent to densely populated areas. Heliyon 9, e15616. https://doi.org/10.1016/j.heliyon.2023.e15616

Wei, T., Hargather, M.J., 2021. A new blast wave scaling Shock Waves (2021) 31:231–238. https://doi.org/10.1007/s00193-021-01012-y

Yang, F., Wang, T., Deng, X., Dang, J., Huang, Z., Hu, S., Li, Y., Ouyang, M., 2021. Review on hydrogen safety issues: Incident statistics, hydrogen diffusion, and detonation process. Int. J. Hydrog. Energy 46, 31467–31488. https://doi.org/10.1016/j.ijhydene.2021.07.005

Zhou, Y., Huang, L., Li, Y., Gao, W., 2024. The prediction model for explosion overpressure in unconfined hydrogen cloud explosion. J. Loss Prev. Process Ind. 88, 105254. https://doi.org/10.1016/j.jlp.2024.105254